

# Microlensing by Stellar Black Holes Around Sgr A\*

Julio Chanamé<sup>1</sup>, Andrew Gould<sup>1,2</sup>, & Jordi Miralda-Escudé<sup>1,3</sup>

<sup>1</sup> *Department of Astronomy, The Ohio State University, Columbus, OH 43210, USA*

<sup>2</sup> *Laboratoire de Physique Corpusculaire et Cosmologie, Collège de France, F-75231, Paris, France*

<sup>3</sup> *Alfred P. Sloan Fellow*

jchaname@astronomy.ohio-state.edu, gould@astronomy.ohio-state.edu,  
jordi@astronomy.ohio-state.edu

## ABSTRACT

We show that at any given time, the Galactocentric black hole Sgr A\* is expected to be microlensing  $N_{\text{lens}} \sim 1.7$  bulge stars if the threshold of detectability of the *fainter* image is  $K_{\text{thr}} = 21$ , and  $N_{\text{lens}} \sim 8$  sources if  $K_{\text{thr}} = 23$ . The lensed images then provide a unique way to detect stellar-mass black holes predicted to cluster around Sgr A\*. If a black hole passes close to a microlensed image, it will give rise to a short (weeks long) microlensing event. We show that the mass and projected velocity of the stellar-mass black hole can both be measured unambiguously from such an event, provided that either a caustic crossing is observed or the astrometric displacement is measured. For  $K_{\text{thr}} = 23$  and moderate magnifications by Sgr A\*, the microlensing event rate from a cluster of 20000 black holes within a radius of 0.7 pc is only  $0.06 \text{ yr}^{-1}$ ; however, if highly magnified images of a star were found, the rate of events by the stellar black holes would be much higher. In addition, the  $N_{\text{lens}}$  sources lensed by Sgr A\* provide a unique probe of extinction *behind* the Galactic center along  $2N_{\text{lens}}$  lines of sight.

*Subject headings:* black hole physics – Galaxy: center – Galaxy: kinematics and dynamics – gravitational lensing

## 1. Introduction

Any black holes formed from the final core collapse of massive stars within the central 5 pc of the Milky Way during the last 10 Gyr should have migrated to the Galactic center

(GC) owing to dynamical friction off ordinary stars (Morris 1993). Miralda-Escudé & Gould (2000, hereafter MG) found that the majority of these black holes survive capture by the massive black hole Sgr A\* and should still be present in the GC today. Low-mass stars older than  $\sim 1$  Gyr should have been expelled from this region by the relaxation process. If stars with an initial mass greater than  $\sim 30 M_{\odot}$  generally produce black holes, then this black-hole cluster should contain about 20,000 members today.

One of the methods to test for the existence of the black-hole cluster is microlensing of a background source, probably a bulge star. This method requires first the discovery of the two images of a bulge star lensed by Sgr A\*, and then the monitoring of these images to detect the short-duration (weeks long) microlensing events caused by the passage of one of the cluster black holes near an image.

The observational challenge here is to identify the two images of a faint ( $K \sim 21$ ) lensed star in a field crowded with  $\sim 400 \text{ arcsec}^{-2}$  stars of similar magnitude and brighter (see § 2.1). Hence, a resolution  $\ll 0''.1$  is required. Such deep, high-resolution observations are beyond current capabilities, but may be achievable with improvements in adaptive optics allowing long exposures, and with NGST. It will then be possible to distinguish the pair of resolved images from the more numerous field stars by means of their positions, flux ratio, colors and proper motions, which are all related. We show in § 2, that there are likely to be a few such detectable image pairs at any given time. However, as we show in § 3, the rate of events caused by cluster black holes is only about 1 per 100 years per image pair, so that still deeper observations will probably be required to detect stellar black holes. In § 4, we show that the masses of these black holes could be measured either by photometric monitoring of a caustic crossing, or from their astrometric effects. Finally, in § 5, we discuss implications of our results.

Alexander & Sternberg (1999) calculated lensing rates for Sgr A\* considered as an isolated body, and obtained results that are broadly consistent with those presented here. The problem of microlensing of background disk sources by stars orbiting near Sgr A\* (similar to the problem we treat here) was investigated by Alexander & Loeb (2001).

## 2. Expected number of stars lensed by Sgr A\*

The expected number of sources being lensed by Sgr A\* at any given time can be estimated empirically given three observational inputs: 1) the  $K$ -band luminosity function (hereafter, LF) of the sources, 2) the volume density of  $K$ -band light as a function of distance behind the GC, and 3) the extinction as a function of distance behind the GC. The first

two of these are well determined from observations, as we summarize below. The last is not measured. For purposes of this paper we will assume that there is no significant additional extinction in the  $\sim 1$  kpc lying behind the GC, above and beyond the  $A_K = 3$  magnitudes of extinction known to lie in front of the GC (e.g., Blum, Sellgren, & DePoy 1996).

## 2.1. Distribution of Stars behind the Galactic Center

We derive the (dereddened) bulge  $K_0$  LF from the  $J$ -band LF measured by Zoccali et al. (2000, hereafter Z00; see their Table 1) using the *Hubble Space Telescope* NICMOS  $J$  and  $H$  images of a field lying at  $(l, b) = (0^\circ, -6^\circ)$  (with a field size  $\Omega_{\text{Zocc}} = 22''.5 \times 22''.5$ ). To obtain the complete  $J$ -band LF, Z00 combined their NICMOS observations, which yield the LF from  $J=16.5$  to  $J=24.5$ , with the bright LF from the Baade’s Window data of Tiede, Frogel, & Terndrup (1995) which extends up to the tip of the red giant branch. We convert the NICMOS part of this LF to  $H_0$  using the reported extinction and observed  $(J, J - H)$  color-magnitude diagram in Z00, and then convert to  $K_0$  using the  $(K, H - K)$  relation observed for nearby main-sequence stars (e.g., Henry & McCarthy 1993). For the bright extension of the LF, we convert to  $K_0$  using the  $(K, J - K)_0$  color-magnitude diagrams reported by Tiede et al. (1995, Figs. 6 and 7). The resulting LF, expressed as the number of stars per square arc minute per  $K$  apparent magnitude (i.e., including our adopted extinction to the GC), is shown in Figure 1. It reaches  $K \sim 26.5$ , and includes bulge main sequence stars with masses  $M \gtrsim 0.15 M_\odot$ . Note that the LF for main-sequence stars is nearly constant throughout the entire bulge (Narayanan, Gould, & DePoy 1996), while luminous stars are more abundant in the GC; hence, this extension of the LF will underestimate the number of lensed luminous stars close to the GC.

EDITOR: PLEASE PLACE FIG. 1 HERE

To convert this to a local *volume density*  $K$  LF,  $(dN/dKdV)(D_s)$ , at a distance  $D_s$  along the line of sight of Sgr A\*, we first write

$$\frac{dN}{dKdV}(D_s) = \frac{\rho(D_s)}{\Sigma_{\text{Zocc}}} \frac{(dN_{\text{Zocc}}/dK_0)|_{K_0=K-\Delta K}}{R_0^2 \Omega_{\text{Zocc}}}, \quad (1)$$

where  $\rho(D_s)$  is the local bulge mass density on the GC line of sight at a distance  $D_s$  from us,  $\Sigma_{\text{Zocc}}$  is the bulge column density toward the Z00 field,  $dN_{\text{Zocc}}/dK_0$  is the number of stars per  $K_0$  magnitude in the Z00 field,  $R_0 = 8$  kpc is the Galactocentric distance,  $\Omega_{\text{Zocc}}$  is the solid angle of the Z00 field,  $\Delta K = A_K(D_s) + 2.5 \log(D_s/R_0)$ , and where we assume  $A_K(D_s) = 3$ . In practice, we set  $\Delta K = A_K = 3$ , thus neglecting the dimming due to larger distances, since this contribution is smaller than the uncertainty introduced by assuming a

constant  $A_K(D_s)$ .

The first factor on the right-hand side of equation (1) depends only on the spatial distribution of the mass in the bulge, and not its normalization. To evaluate it, we use a combination of the Kent (1992) model, which is based on K band images, and the DIRBE data from Dwek et al. (1995). The reason this combination is required is that the Kent model is axisymmetric, and so does not include the effects of the bar which are important at large radius, while the DIRBE map cannot be applied at small radius because of its limited resolution. We rewrite this term as

$$\frac{\rho(D_s)}{\Sigma_{\text{Zocc}}} = \frac{\rho(D_s)}{\Sigma_{(0,-2)}} \frac{\Sigma_{(0,-2)}}{\Sigma_{\text{Zocc}}}, \quad (2)$$

where  $\Sigma_{(0,-2)}$  is the column density in the direction  $(l, b) = (0, -2^\circ)$ . We determine the first ratio from equation (3) in Kent (1992), except that we impose a constant density core within 0.7 pc due to relaxation effects around Sgr A\* (MG). We determine the second ratio from the DIRBE map (Fig. 1a in Dwek et al. 1995), obtaining a value  $\Sigma_{(0,-2)}/\Sigma_{\text{Zocc}} \simeq 13$ . Note that this procedure is relatively insensitive to possible disk contamination of the Z00 field since to leading order this contamination affects both the star counts and the DIRBE map equally. We have also used this same procedure to predict the surface density of stars near Sgr A\*, which is found to be 440 arcsec<sup>-2</sup> stars with  $K < 21$  mag, and about 1000 arcsec<sup>-2</sup> with  $K < 23$  mag.

## 2.2. Number of Lensed Sources

The two images of a microlensed source will have magnifications given by

$$A_{\pm}(u) = \frac{u_{\pm}^2}{u_+^2 - u_-^2}, \quad u_{\pm} = \frac{u \pm \sqrt{u^2 + 4}}{2}, \quad u \equiv \frac{\theta_{\text{rel}}}{\theta_{\text{E}}}, \quad (3)$$

where  $\theta_{\text{rel}}$  is the angular separation of the lens and source,  $\theta_{I\pm} = u_{\pm}\theta_{\text{E}}$  are the positions of the two images,  $\theta_{\text{E}}$  is the Einstein radius,

$$\theta_{\text{E}}(D_s) = \sqrt{\frac{4GM_*}{c^2} \frac{D_{ls}}{D_l D_s}} = 0.''55 \left( \frac{10D_{ls}}{D_s} \right)^{1/2}, \quad (4)$$

$M_* = 3 \times 10^6 M_{\odot}$  is the mass of Sgr A\*,  $D_l = R_0$ ,  $D_s$  is the distance to the source, and  $D_{ls} = D_s - D_l$ . The angular separation of the two lensed images of a background star at  $D_{ls} \sim 1$  kpc is  $\sim 2\theta_{\text{E}} \sim 1''$ , clearly large enough to resolve them. On the other hand, the duration of the “microlensing event” is very long, given the typical proper motion of bulge stars of a few mas per year. This implies that the usual method of microlensing detection from the

magnification lightcurve is impractical. Thus, to detect a lensed source, it is essential to identify *a pair of images*, which can be done from their relative magnifications and proper motions (both of which are unambiguously predicted from their positions relative to Sgr A\*), as well as their common dereddened color.

The expected number of observable lenses  $N_{\text{lens}}$  is simply the number for which the fainter image is brighter than the threshold of detectability,  $K_{\text{thr}}$ ,

$$N_{\text{lens}} = \int_{R_0+0.7 \text{ pc}}^{D_{s,\text{max}}} dD_s D_s^2 \int_0^\infty d\theta 2\pi\theta \frac{dN}{dV} \left[ D_s, K_{\text{thr}} + 2.5 \log A_- \left( \frac{\theta}{\theta_E(D_s)} \right) \right], \quad (5)$$

where  $dN/dV(D_s, K') = \int^{K'} dK (dN/dV dK)(D_s, K)$  is the cumulative LF. We use  $D_{s,\text{max}} = 9$  kpc, effectively assuming that additional obscuration becomes important farther than 1 kpc behind the GC. We find for  $K_{\text{thr}} = (21, 22, 23)$ , that  $N_{\text{lens}} = (1.7, 3.8, 8.0)$ , which can be summarized,

$$N_{\text{lens}} \simeq 8 \times 10^{0.33(K_{\text{thr}}-23)}, \quad (21 < K_{\text{thr}} < 23). \quad (6)$$

Thus, in order to have a reasonable probability of finding one lensed star, the inner 1'' of the GC must be imaged down to at least  $K \sim 21$ . Once a lensed image pair is detected, it is mainly the brighter member that will be useful to search for black-hole cluster members. Figure 1 shows the distribution of brighter and fainter members (solid and dashed lines, respectively) for the three cases  $K_{\text{thr}} = (21, 22, 23)$ . From 0.7 pc and up to 1 kpc behind the GC the contributions of equal logarithmic intervals of  $D_{ls}$  are 24%, 31%, and 45%. Therefore, although most lensed sources will be from the ‘‘outer’’ bulge, with  $\theta_E \gtrsim 0''.1$ , a significant fraction will be close to Sgr A\*, with  $\theta_E \sim 30$  mas ( $\sim 250$  AU), corresponding to  $D_{ls} \sim 3$  pc. Hence, detection of these images, at  $\theta_E \sim 30$  mas, might be compromised by extra extinction or emission from an accretion flow/disk around Sgr A\*.

In the above calculations it has been assumed that there is essentially no extra extinction in the 1 kpc behind the GC. In fact, most of the extinction measured towards the GC is thought not to arise in the immediate vicinity of the Galactic center, but several kpc away, in a ring of molecular material. If this holds behind the GC as well, then our results for  $N_{\text{lens}}$  are not affected. On the other hand, if the situation behind the GC is different than in front of it, there are two possibilities. First, if, say,  $A_K = 1$  magnitude of extinction is uniformly distributed across the first kpc behind, then the closer sources will be the main contributors to  $N_{\text{lens}}$ , and the numbers quoted in equation (6) would be reduced by about 30-40%. A second possibility is that the extra extinction is concentrated close to the GC, in which case all the sources behind are equally affected. Hence, if there is 1 mag of extra extinction close to the GC, then the quoted numbers for  $N_{\text{lens}}$  would be for  $K_{\text{thr}} = (22, 23, 24)$ , instead of (21, 22, 23). The detection of lensed sources will itself allow a quantitative probe of extinction behind the GC, as we discuss in § 5.

In Figure 2 we show as solid lines the shear distribution ( $dN/d\gamma$ ) of the brighter pair member obtained for the three magnitude limits. Pairs with high magnifications (shear close to unity) are less numerous than those with small magnifications. The area under any of these curves corresponds to the number of lensed pairs that are expected to be found at the corresponding detection threshold. The solid line in the left hand panel of Figure 3, below, shows  $N(> \gamma)$ , the cumulative distribution of  $\gamma$  of the brighter pair member, for the case  $K_{thr} = 23$ .

EDITOR: PLEASE PLACE FIG. 2 HERE

### 3. Rate of Microlensing Events by the Cluster Black Holes

After two images of a background bulge star lensed by Sgr A\* have been identified, monitoring them could reveal short microlensing events due to one of the cluster black holes passing near one of the images. If the typical cluster black hole has a mass comparable to the masses inferred from X-ray binary systems,  $m_{bh} \simeq 7 M_{\odot}$  (Bailyn et al. 1998), the mass ratio of the binary lens of Sgr A\* and the cluster black hole is  $q = m_{bh}/M_* \sim 2 \times 10^{-6}$ . The lightcurves would be similar to those caused by planets around ordinary stars (Mao & Paczyński 1991; Gould & Loeb 1992; Albrow et al. 1998), although with longer timescales. In this section, we calculate the rate at which these planet-like events should take place.

The rate of microlensing due to cluster black holes depends on their surface density, their velocity distribution, and a *linear cross section* giving the size of the region around an unperturbed image where a cluster black hole will significantly change its magnification. We obtain the surface density of black holes,  $\Sigma_{\bullet}(b)$  (where  $b$  is the projected radius), using the model in MG, where the cluster density varies as  $\rho(r) \propto r^{-7/4}$ , the total stellar mass enclosed within  $r_0 = 1.8$  pc is equal to  $M_* = 3 \times 10^6 M_{\odot}$ , and the density normalization of the black hole cluster is reduced by a factor  $(m_{bh}/\bar{m})^{-1/2} = 0.18$  below that of the cluster of stars, owing to the change in the mean mass of the objects between the black hole cluster ( $m_{bh} \sim 7 M_{\odot}$ ) at  $r \lesssim 0.7$  pc and the stellar cluster at larger distances ( $\bar{m} \sim 0.23 M_{\odot}$ ). At projected radii  $b \ll 0.7$  pc, the result is

$$\Sigma_{\bullet}(b) = 0.18 \frac{5}{16\pi} \frac{M_*/m_{bh}}{r_0^{5/4}} \int_{-\infty}^{\infty} (z^2 + b^2)^{-7/8} dz = 1.6 \times 10^5 \left(\frac{\theta}{1''}\right)^{-3/4} \text{pc}^{-2}, \quad (7)$$

where  $\theta \equiv b/R_0$  is the angular distance from the center.

We note here that the reduction factor  $(m_{bh}/\bar{m})^{-1/2} = 0.18$  probably gives us an underestimate of the surface density of lensing objects, because the time necessary for the black

hole cluster to expand and achieve equilibrium under relaxation with the low-mass stars is somewhat longer than the age of the universe (this was not taken into account in MG). This means that the rate of events we will find may be underestimated, proportionally to the surface density. This issue will be addressed in a future paper.

We assume an isotropic velocity distribution. For  $\rho(r) \propto r^{-7/4}$ , the Jeans equation (see Binney & Tremaine 1987) yields a one-dimensional velocity dispersion  $\sigma(r) = \sqrt{4/11} v_c(r) = 68.5(r/\text{pc})^{-1/2} \text{ km s}^{-1}$ , where  $v_c(r)$  is the circular velocity. The projected two-dimensional velocity dispersion is  $\sigma_p(b) = 0.99\sigma(b) = 68(b/\text{pc})^{-1/2} \text{ km s}^{-1}$ .

We calculate the linear cross section assuming a Chang-Refsdal lens (Chang & Refsdal 1979; Schneider, Ehlers & Falco 1992), of a point mass in the external shear  $\gamma = (\theta_E/\theta_I)^2$  caused by Sgr A\*, where  $\theta_I$  is the angular distance from the image to Sgr A\*. We first consider events on the brighter member of the unperturbed pair, with unperturbed magnification  $A_+$  given by equation (2). We will later include the contribution from the fainter images. Our criterion for the detectability of the short microlensing event is that the magnification of this image is increased to at least  $(1 + \delta)A_+$ . If  $\xi$  is the axis joining Sgr A\* and the cluster black hole, and  $\eta$  the perpendicular axis, we find that the contours of constant  $\delta$  in the source plane have lengths along the  $(\xi, \eta)$  axes of

$$L_\xi = \frac{2(2\gamma - \lambda + 1)}{\sqrt{\lambda - \gamma}} \sqrt{q} R_0 \theta_E, \quad L_\eta = \frac{2(2\gamma + \lambda - 1)}{\sqrt{\lambda + \gamma}} \sqrt{q} R_0 \theta_E, \quad (8)$$

where

$$\lambda = \left( 1 - \frac{1}{(1 + \delta)A_+} \right)^{1/2}. \quad (9)$$

We first consider the case  $\lambda = 1$ , which corresponds to requiring a caustic crossing (i.e.,  $\delta = \infty$ ).

To compute the rate of events, we notice first that the surface density of caustics in the source plane is  $\Sigma_\bullet/(1 - \gamma^2)$ , and the velocity dispersion of these caustics is anisotropic. To render the calculation more transparent, it is convenient to make a linear transformation of the source plane to  $\xi' = \xi/(1 + \gamma)$ , and  $\eta' = \eta/(1 - \gamma)$  (this transformation would be locally equivalent to the lens plane in the absence of the perturbing black hole). In this transformed source plane, the surface density and velocity dispersion of the caustics are the same as the surface density and velocity dispersion of the black holes in the lens plane, and the dimensions of contours of constant  $\delta$  are modified to  $L_{\xi'} = L_\xi/(1 + \gamma)$ ,  $L_{\eta'} = L_\eta/(1 - \gamma)$ .

The rate of events for a given unperturbed image is just the product  $\omega = \Sigma_\bullet \sigma_p \bar{L}'$ , where  $\bar{L}'$  is the average length of the  $\delta$  contour over all possible directions of motion of the black hole, and where  $\Sigma_\bullet$  and  $\sigma_p$  are evaluated at the projected radius of the brighter unperturbed

image,  $b = \gamma^{-1/2} R_0 \theta_E$ . In the case  $\delta = \infty$ ,  $\bar{L}'$  can be evaluated by noticing that, because the shape of the caustic is always concave between cusps, the cross section for any angle of motion is determined solely by the position of the four cusps. If  $\alpha$  is the angle of the motion relative to the  $\xi'$  axis, the cross section is  $L_{\xi'} \cos \alpha$  for  $\alpha < \alpha_c$ , and  $L_{\eta'} \sin \alpha$  for  $\alpha > \alpha_c$ , where  $\tan \alpha_c = L_{\xi'}/L_{\eta'}$ . Hence,

$$\bar{L}' = \frac{2}{\pi} \left( \int_0^{\alpha_c} L_{\xi'} \cos \alpha \, d\alpha + \int_{\alpha_c}^{\pi/2} L_{\eta'} \sin \alpha \, d\alpha \right) = \frac{2}{\pi} \sqrt{L_{\xi'}^2 + L_{\eta'}^2} = \frac{8\sqrt{2}\gamma}{\pi(1-\gamma^2)} \sqrt{q} R_0 \theta_E. \quad (10)$$

This yields an event rate

$$\omega = 1.2 \times 10^{-2} \frac{\gamma^{13/8}}{1-\gamma^2} \left( \frac{\theta_E}{1''} \right)^{-1/4} \text{yr}^{-1}. \quad (11)$$

For a bulge star at  $D_{ls}=500$  pc (i.e.,  $\theta_E \simeq 0''.4$ ), a shear of  $\gamma=0.6$  (i.e., impact parameter  $u=0.52$ ,  $A_+=1.56$ ), this implies approximately 0.01 microlensing events per year on the brighter image. If a very highly magnified pair of images is found, the rate of events is enhanced. For example, for  $\gamma = 0.97$ , when the brighter image has an unperturbed magnification of 17, the rate is enhanced to  $\sim 0.25$  events per year (an event like this would last for 2 months, while the total Sgr A\* event has an Einstein radius crossing time of 100 years).

We can now compute the rate of events as a function of  $\gamma$ , by multiplying the mean number of images lensed by Sgr A\* (which is shown as the solid lines in Figure 2) times the event rate on a given image from equation (11). The result is shown as the dashed line in Figure 2. The cumulative event rate is shown in the left hand panel of Figure 3 as the dashed curve. A large fraction of the mean rate of events occur on high magnification images. The mean rate of events (integrated over  $\gamma$ ) is (0.012, 0.021, 0.034)  $\text{yr}^{-1}$ , for  $K_{thr}=(21, 22, 23)$ , respectively. However, the actual expected rate depends strongly on whether images of high  $\gamma$  (lensed by Sgr A\*) are found. For example, the expected number of lensed images for  $K_{thr} = 23$  is 8, of which an average of 1 has  $\gamma > 0.7$ , and two thirds of the stellar black hole events are contributed by images with  $\gamma > 0.7$ .

EDITOR: PLEASE PLACE FIG. 3 HERE

So far, we have calculated only the rate of *caustic crossing* microlensing events. In fact, many events can be detected that do not cross the caustic, although as we discuss in § 4, the interpretation of these may be more difficult. The precise requirement for detection will depend on the precision with which the flux from these faint images could be monitored. For illustration, the dotted line in Figure 4 shows the rate of events  $\Gamma(\gamma)$  for  $\delta = 1$  (i.e., when the unperturbed image is required to be magnified by a factor of at least 2 relative to its

magnification due to Sgr A\* only), compared to  $\delta = \infty$ , for  $K_{thr} = 23$ . The total rates are almost doubled, to (0.022, 0.038, 0.062) yr<sup>-1</sup>, for  $K_{thr}=(21, 22, 23)$ .

EDITOR: PLEASE PLACE FIG. 4 HERE

The characteristic timescale of the events is  $\Delta t \sim (0.5 L_{\xi'} L_{\eta'}) / (2 \bar{L}' \sigma_p)$ , so for caustic crossing we obtain

$$\Delta t \sim 68 \frac{\gamma^{3/4}}{(1 - \gamma^2)^{1/2}} \left( \frac{\theta_E}{1''} \right)^{3/2} \left( \frac{m_{bh}}{7 M_\odot} \right)^{1/2} \text{ days.} \quad (12)$$

With  $\gamma = 0.6$  and  $\theta_E \simeq 0''.4$ , this gives an event duration of  $\sim 2$  weeks. High magnification events last longer, taking  $\sim 2$  months to complete a  $\gamma = 0.97$  event.

The Chang-Refsdal approximation used here is potentially subject to severe problems when approaching the limit of very high magnifications ( $\gamma \rightarrow 1$ ). This is because there is a point where the caustics become so large that they begin to overlap, so that we reach the “optically thick” lensing regime in which several cluster black holes are significantly affecting the magnification of the unperturbed image at the same time. Also the caustics weaken in this regime, so that when the finite size of the source is taken into account, the caustic crossing may be difficult to detect. We estimate this to happen at  $\gamma \simeq 0.98$  (at which  $\omega \Delta t \simeq 0.1$ ). The vertical dotted line in the left hand panel of Figure 3 marks this point, beyond which the contribution to the rate is only  $\sim 8\%$  of the total. While images of background sources highly magnified by Sgr A\* are easier to identify, the interpretation of microlensing events on such images gets complicated because of the merging of separated caustics. Hence it is desirable to wait for the identification of a lensed image pair and then, if the corresponding shear is in this regime, work the actual case through more carefully.

In our calculation of the rate of events we have so far considered only the brighter image of each pair of stars lensed by Sgr A\*. Figure 2 shows that high magnification pairs, though rare, dominate the rate of microlensing events. One can see from Figure 3 that approximately 50% of the total rate comes from images with  $\gamma > 0.8$ , for which the ratio of their magnifications to that of their corresponding fainter images is  $\mathcal{R} = 1/\gamma^2 < 1.56$ . Thus, the events on the fainter image should be of comparable importance. The precise calculation of the cross section for the fainter images is more difficult because the caustics have a different morphology for  $\gamma > 1$  (two triangles) than for  $\gamma < 1$  (one quadrilateral). However, for  $\gamma \rightarrow 1$  (which is of relevance here), the combined cross section of the two triangles is very well approximated by that of a single quadrilateral with total extent equal to that of the two triangles (see Schneider, Ehlers, and Falco, 1992, p. 259). We therefore calculate the rate using this approximation and find, for events on the fainter images, (0.008, 0.015, 0.024) yr<sup>-1</sup>, for  $K_{thr}=(21, 22, 23)$  respectively. We show the result for  $K_{thr}=23$  in the right panel

of Figure 3.

#### 4. Measuring the Black Hole Masses

The stellar black holes have masses much smaller than that of Sgr A\*, and so are formally identical to planetary lenses. In the case of planetary systems, the orbital velocity of the planet is usually negligible compared to the relative velocity of the lens and the source, and so the mass ratio can be determined from the lightcurve alone by measuring the ratio of timescales of the planetary perturbation and the entire event (Gould & Loeb 1992). However, in the present case the orbiting black holes have speeds that are the same order or larger than the sources being lensed.

It is nevertheless often possible to recover the black-hole mass. For caustic-crossing events, this can be done just from photometry. In principle, the black-hole mass can also be recovered astrometrically, both for caustic-crossing and non-caustic crossing events. However, for non-caustic crossers, this determination will prove difficult in practice.

First, note that the normalized lens-source separation,  $u$ , can be determined either from the flux ratio  $\mathcal{R}$  of the two images,  $u = \mathcal{R}^{1/4} - \mathcal{R}^{-1/4}$ , or from the measured fractional offset  $\Delta \equiv (\theta_{I+} + \theta_{I-})/(\theta_{I+} - \theta_{I-})$  of Sgr A\* from the midpoint of the two images,  $u = 2(1/\Delta - 1)^{-1/2}$ . One can then determine the Einstein radius,  $\theta_E = (\theta_{I+} - \theta_{I-})/(\mathcal{R}^{1/4} + \mathcal{R}^{-1/4})$ , or  $\theta_E = \sqrt{\Delta^{-1} - \Delta}(\theta_{I+} - \theta_{I-})/2$ . From the known mass of Sgr A\*, this then determines the distance to the source. Next, the shear  $\gamma = \mathcal{R}^{-1/2}$  or  $\gamma = (1 - \Delta)/(1 + \Delta)$  determines the geometry of the Chang-RRefsdal lens, up to an overall scale factor  $q^{1/2}$  (proportional to the size of the caustic). The source speed is known from the proper motion of the major image across the sky, thus, the only two unknowns are the velocity of the lens (which determines how fast the caustic moves over the source), and the size of the caustic, related to the mass of the lens. Measuring the mass of the lens is the crucial step required to prove that a microlensing event is caused by a stellar black hole.

If the source passes through the caustic, then its trajectory can be determined from the photometric light curve. This will be much easier for black-hole caustics than for caustics that have been analyzed in binary-lens events to date (e.g., Afonso et al. 2000), because, as mentioned above, the geometry of the caustic is already known up to a scale factor  $q^{1/2}$ . The ratio of the angular size of the caustic to the angular radius of the source can then be determined from the duration of the caustic crossing (e.g., Afonso et al. 2000; Albrow et al. 1999, 2000, 2001). If the dereddened color and magnitude of the source is measured (e.g., from *JHK* photometry), then the angular size of the source can be determined from the

color/surface-brightness relation (e.g., van Belle 1999). Even with just  $HK$  photometry, a good estimate can be made because, for fixed apparent color and magnitude, the inferred source size depends only weakly on the reddening. It may not be possible to obtain  $H$  photometry for these very faint stars; however, the sources at the faint magnitudes at which we expect to find lenses should be main-sequence stars, and since their distance will be known, it should be possible to estimate their angular size even with only the  $K$  magnitude. Finally, since  $\gamma$  is known, the ratio of the angular size of the caustic to  $\theta_E$  immediately gives the mass ratio,  $q$ .

Astrometry provides an independent method to determine  $q$  for both caustic and non-caustic crossing events. For fixed source trajectory through this geometry, the astrometric deviation is proportional to  $q\theta_E$ . Hence, if this trajectory were known, then measurement of the astrometric deviation would yield  $q$ .

As discussed above, if the source passes through the caustic, then the trajectory can be easily determined from the photometric light curve alone. However, if the source passes outside a cusp, the photometric light curve is potentially subject to two interpretations: the approached cusp could be along the Sgr-A\*/black-hole axis, or perpendicular to it. These two cases are nevertheless easily resolved astrometrically since the two astrometric deviations are at right angles to one another. Once it is resolved, one knows from the height of the photometric peak of the deviation, how close the source was to the cusp when it crossed the cusp axis. The astrometric deviation at this point then gives  $q$ .

For caustic-crossing events the astrometric deviation is of order  $q\theta_E \sim 1.5 \text{ mas}(\theta_E/1'')$ . Recall that just to resolve the imaged stars requires *resolution*  $\ll 0''.1$ , so *centroiding* the images to sub-mas levels should be challenging but perhaps feasible. However, in the limit of  $\gamma \ll 1$  (which dominates the expected distribution of lenses shown in Fig. 2), the maximum astrometric deviation is  $q\theta_E/\sqrt{8}$ . This factor  $\sim 3$  reduction relative to the caustic-crossing case could render an already difficult measurement impossible.

## 5. Discussion

We have shown that a pair of lensed images from a background bulge star is likely to be found by the time stars are imaged down to  $K = 21$  within an arc second of Sgr A\*, and about 8 pairs are expected if  $K = 23$  is reached. These images will need to be distinguished from the much more numerous stars in the vicinity of Sgr A\* by finding a pair of images with the correct relations between magnifications, positions and proper motions expected for a point mass lens.

The detection of these lenses would show that Sgr A\* is concentrated within a radius  $\lesssim 1''$ , but this has already been demonstrated at much smaller radii by the direct measurement of stellar accelerations (Ghez et al. 2000). A much more interesting application would be to test the predicted presence of a cluster of stellar black holes around Sgr A\*. Unfortunately, we find that these events should be quite rare: only about one caustic-crossing event per century for every lensed image that is monitored. However, this rate would be enhanced if a pair of highly magnified images were found.

If an event is detected toward the black-hole cluster, it need not necessarily be due to a black hole: there will also be events in this direction caused by ordinary stars around the black-hole cluster. Assuming a core radius of  $r_c = 0.7$  pc for the old population of low-mass stars (caused by scatterings from the cluster black holes), the surface mass density of these stars is a factor  $(R_0\theta_E/r_c)^{3/4}/0.18 \simeq 0.45(\theta/0.''5)^{3/4}$  smaller than that of the black holes. The duration of these events due to old stars would be similar to the ones from the cluster black holes, since the lower masses are roughly compensated by the lower velocity dispersion. However, as discussed in § 4, they could be distinguished by photometric monitoring of a caustic crossing and/or astrometrically.

Alexander & Loeb (2001) have also investigated microlensing by stellar objects near Sgr A\*. In their case, they consider background disk stars as sources (whereas we have considered bulge stars), and they assume that a population of  $1M_\odot$  stars surrounds Sgr A\*, with a density profile  $\rho \propto r^{-3/2}$ . They discuss the increased likelihood to observe a star with high magnification when considering the microlensing by stellar objects near the Einstein radius of Sgr A\*.

We note that more microlensing events by cluster black holes might be found by monitoring to the same depth all the stars over the entire area of the black hole cluster, within  $\sim 20''$  of Sgr A\*. In this case, we would not know a priori which of the source stars are at a large distance behind the GC, and the magnification by Sgr A\* would be negligible. The events from the cluster black holes would tend to have Einstein timescales  $t_E$  that were  $(m_{\text{bh}}/\bar{m})^{1/2} \sim 6$  times longer than those of ordinary bulge events (since, far away from Sgr A\*, the velocities of the black holes are similar to those of other bulge stars). They could not be unambiguously distinguished on the basis of timescales alone because the full-width at half-maximum of the mass estimate is almost a factor 100 (Gould 2000). However, since most of this width is due to the large dispersion in proper motions  $\mu$ , it could largely be removed by measuring the astrometric deviation, which yields the Einstein radius  $\theta_E$ , and so  $\mu = \theta_E/t_E$ . Since the surface density of black holes is  $\Sigma_\bullet \propto \theta^{-3/4}$ , and their velocity dispersion  $\sigma \propto \theta^{-1/2}$ , the number of microlensing events they produce within  $\theta$  is proportional to  $\theta^{3/4}$ , so there should be about 10 times more events from the entire cluster, within  $20''$ ,

than events that are affected by the magnification of Sgr A\*.

Finally, we point out a very interesting additional application of the lensed pairs that we predict should be found at any detection limit: they are potentially powerful probes of the extinction immediately behind the GC, which is the difference between the extinction toward the source, and the extinction toward GC sources along the same line of sight as the images. As we discuss immediately below, the former can be determined by obtaining multi-color photometry of both images and spectroscopy of the brighter one. The latter can be found from the distribution of colors and magnitudes of sources along lines of sight neighboring the images, the great majority of which lie within  $\lesssim 1$  pc of the GC. Recall from § 4, that  $\theta_E$  can be determined from the measured image positions, which implies that  $D_{ls}$ , the source distance behind the GC, is known from equation (4).

To accurately measure the extinction to the source, its intrinsic color must be determined. This can best be done by spectroscopy of the brighter image. A large fraction of the lensed sources have small  $\gamma$  (see Fig. 2), and so consist of a luminous source whose brighter image is weakly magnified, and whose fainter image is heavily demagnified. Hence the brighter image must have  $K \leq K_{\text{thr}} + 5 \log \gamma$ . Thus, these low- $\gamma$  image pairs, which contribute almost nothing to the probability of detecting cluster black holes, are the best probes of extinction. See Figure 1 for the overall distribution of brighter images. For cases where the brighter image is sufficiently faint, spectroscopy will no longer be possible, and it will be necessary to determine the intrinsic color from multi-color photometry. This will be less accurate, but probably still useful. Of course, once the intrinsic color of the source is known from measurements of the brighter image, extinction can be measured along *both* lines of sight to the source, by measuring the apparent colors of both images.

JC thanks Scott Gaudi for useful discussions and insights. Work by AG was supported in part by grant AST 97-27520 from the NSF, and in part by a grant from Le Ministère de L'Éducation Nationale de la Recherche et de la Technologie.

## REFERENCES

- Albrow, M. et al. 1998, ApJ, 509, 687  
 Albrow, M. et al. 1999, ApJ, 522, 1011  
 Albrow, M. et al. 2000, ApJ, 534, 894  
 Albrow, M. et al. 2001, ApJ, 549, 759

- Alexander, T., & Loeb, A. 2001, ApJ, 551, 223
- Alexander, T., & Sternberg, A. 1999, ApJ, 520, 137
- Afonso, C. et al. 2000, ApJ, 532, 340
- Bahcall, J.N. 1984, ApJ, 287, 926
- Bailyn, C.D., Jain, R.K., Coppi, P., & Orosz, J.A. 1998, ApJ, 499, 367
- Binney, J., & Tremaine, S. 1987, Galactic Dynamics (Princeton: Princeton University Press)  
210
- Blum, R.D., Sellgren, K., & DePoy, D.L. 1996, ApJ, 470, 864
- Chang, K., & Refsdal, S. 1979, Nature, 282, 561
- Dwek, E., Arendt, R.G., Hauser, M.G., Kelsall, T., Lisse, C.M., Moseley, S.H., Silverberg,  
R.F., Sodroski, T.J., & Weiland, J.L. 1995, ApJ, 445, 716
- Genzel, R., Pichon, C., Eckart, A., Gerhard, O.E., & Ott, T. 2000, MNRAS, 317, 348
- Ghez, A.M., Morris, M., Becklin, E.E., Tanner, A., & Kremenek, T. 2000, Nature, 407, 349
- Gould, A. 2000, ApJ, 535, 928
- Gould, A., & Loeb, A. 1992, ApJ, 396, 104
- Henry, T.J., & McCarthy, D.W., Jr. 1993, AJ, 106, 773
- Kent, S.M. 1992, ApJ, 387, 181
- Mao, S., & Paczyński, B. 1991, ApJ, 374, L37
- Miralda-Escudé, J., & Gould, A. 2000, ApJ, 545, 847 (**MG**)
- Morris, M. 1993, ApJ, 408, 496
- Narayanan, V.K., Gould, A., & Depoy, D.L. 1996, ApJ, 472, 183
- Schneider, P., Ehlers, J., & Falco, E.E. 1992, Gravitational Lenses (Berlin: Springer)
- Tiede, G.P., Frogel, J.A., & Terndrup, D.M. 1995, AJ, 110, 2788
- van Belle, G.T. 1999, PASP, 111, 1515

Zoccali, M., Cassisi, S., Frogel, J. A., Gould, A., Ortolani, S., Renzini, A., Rich, R. M., & Stephens, A. 2000, *ApJ*, 530, 418 (**Z00**)

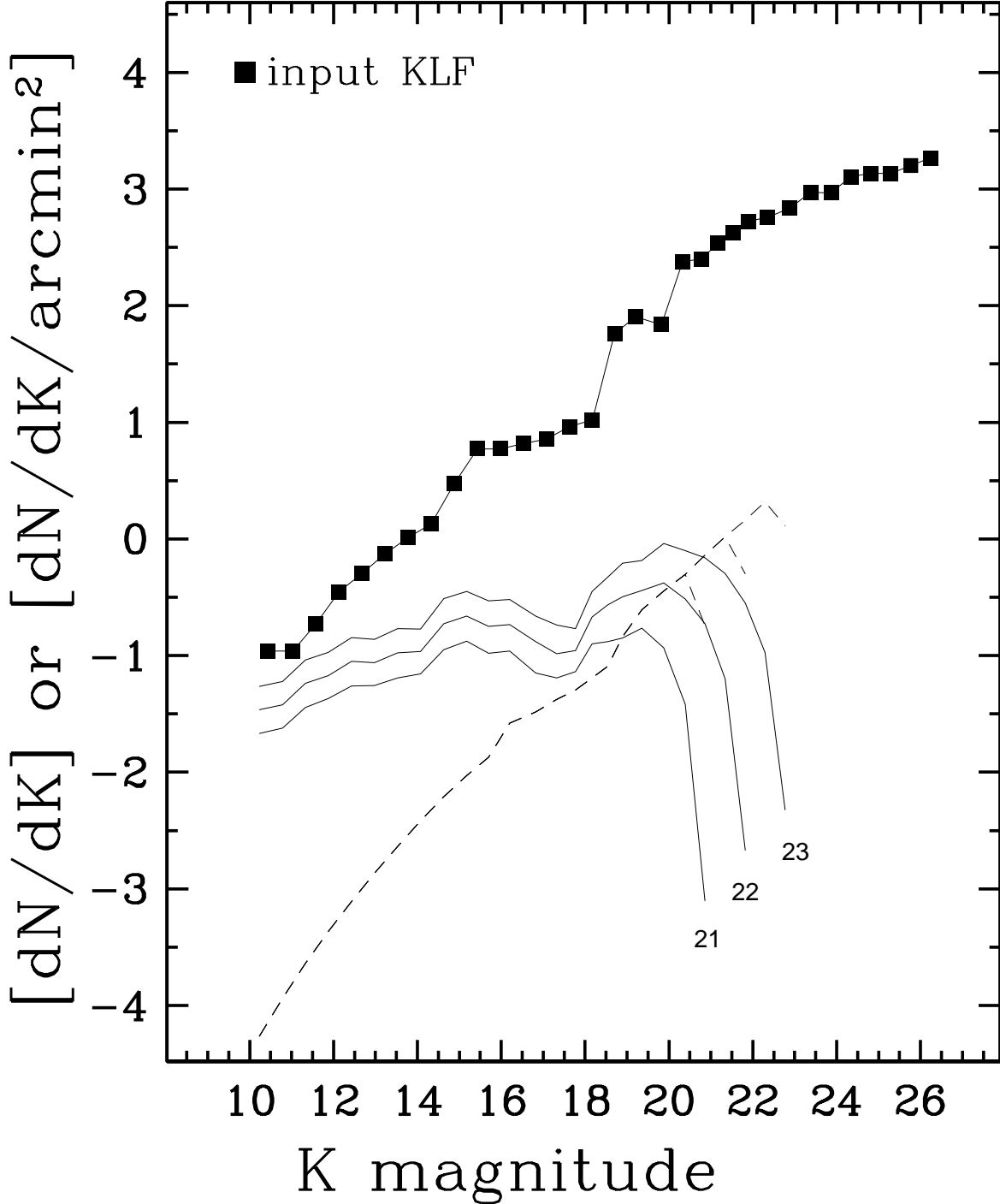


Fig. 1.— The extinguished surface density  $K = K_0 + A_K$  luminosity function  $[dN/dK/\text{arcmin}^2]$  derived from the Zoccali et al. (2000) data is shown as filled squares. The estimated GC extinction  $A_K = 3$  has been added to facilitate direct comparison with the other curves, which all assume this extinction. Solid lines represent the number of brighter images per magnitude  $[dN/dK]$  of bulge stars lensed by Sgr A\* for three detection thresholds. Similarly, the dashed lines represent the corresponding distributions of the fainter images.

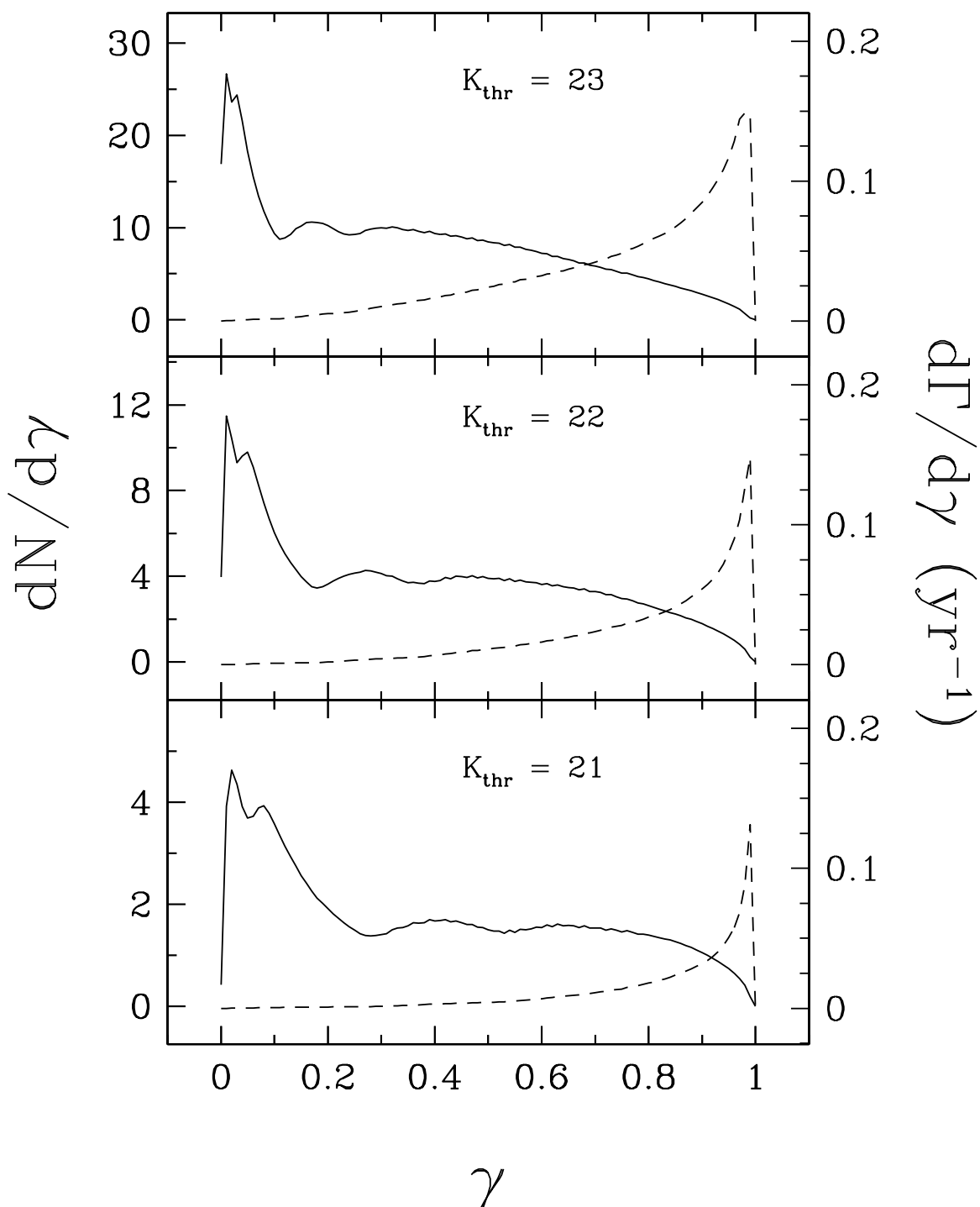


Fig. 2.— The distributions of the detectable number of sources lensed by Sgr A\* as a function of the shear  $\gamma$  (solid lines), and of the rate of microlensing events produced by the cluster black holes,  $d\Gamma/d\gamma$  (dashed lines), for the three magnitude thresholds mentioned in the text. Note that  $d\Gamma/d\gamma = \omega(\gamma) \cdot dN/d\gamma$ , where  $\omega(\gamma)$  is given by eq. (11).

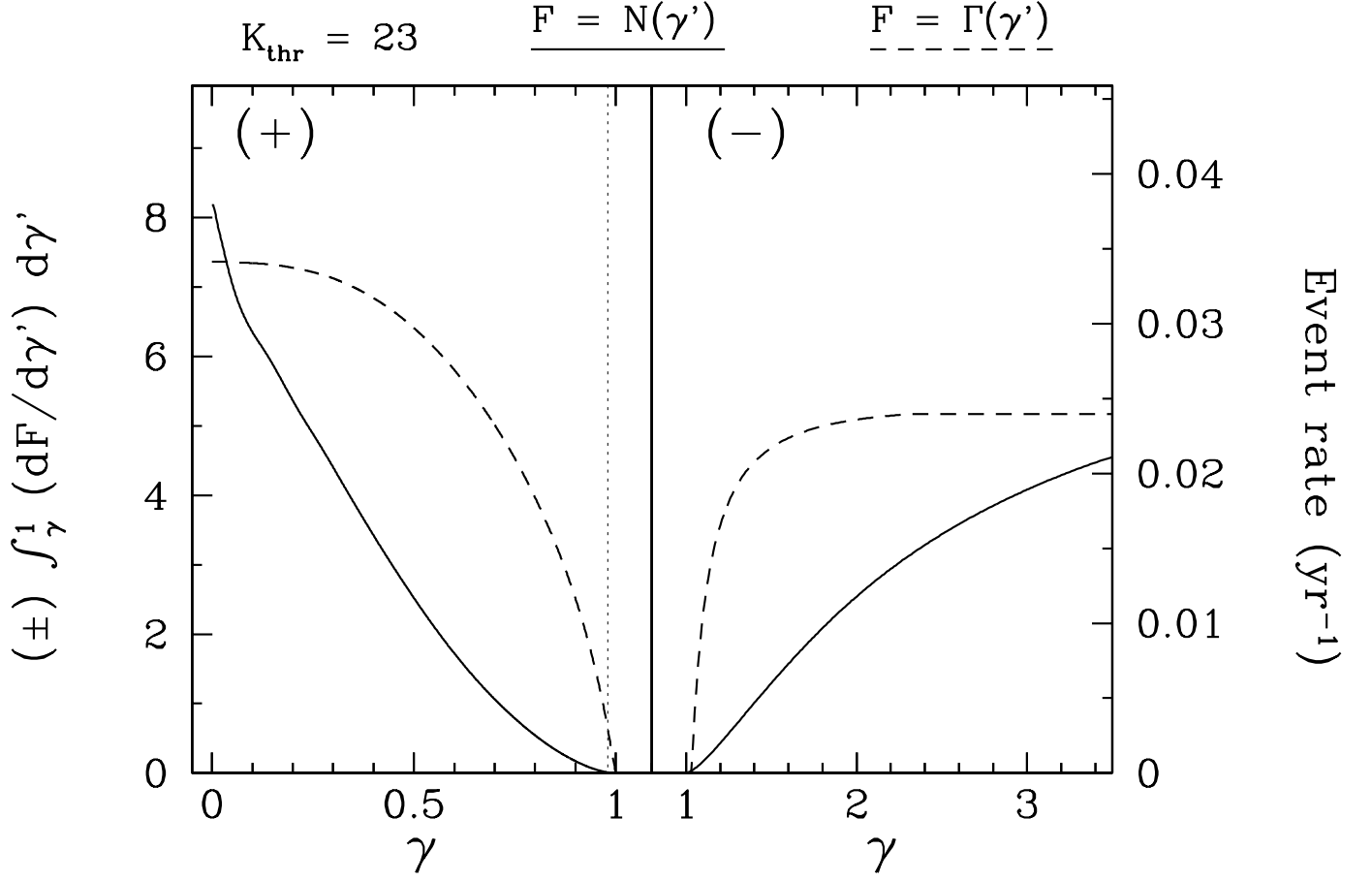


Fig. 3.— Cumulative shear distributions of the number of sources lensed by Sgr A\* (solid lines) and of the rate of microlensing events (dashed lines), for a magnitude limit of  $K_{\text{thr}} = 23$ . The left panel corresponds to the brighter pair members, and the right panel to the fainter ones. The (plus or minus) sign between parenthesis in each panel indicates the corresponding sign of the integral in the left-hand vertical label. The vertical dotted line in the left panel marks the point where the Chang-Refsdal approximation begins to break down (see text).

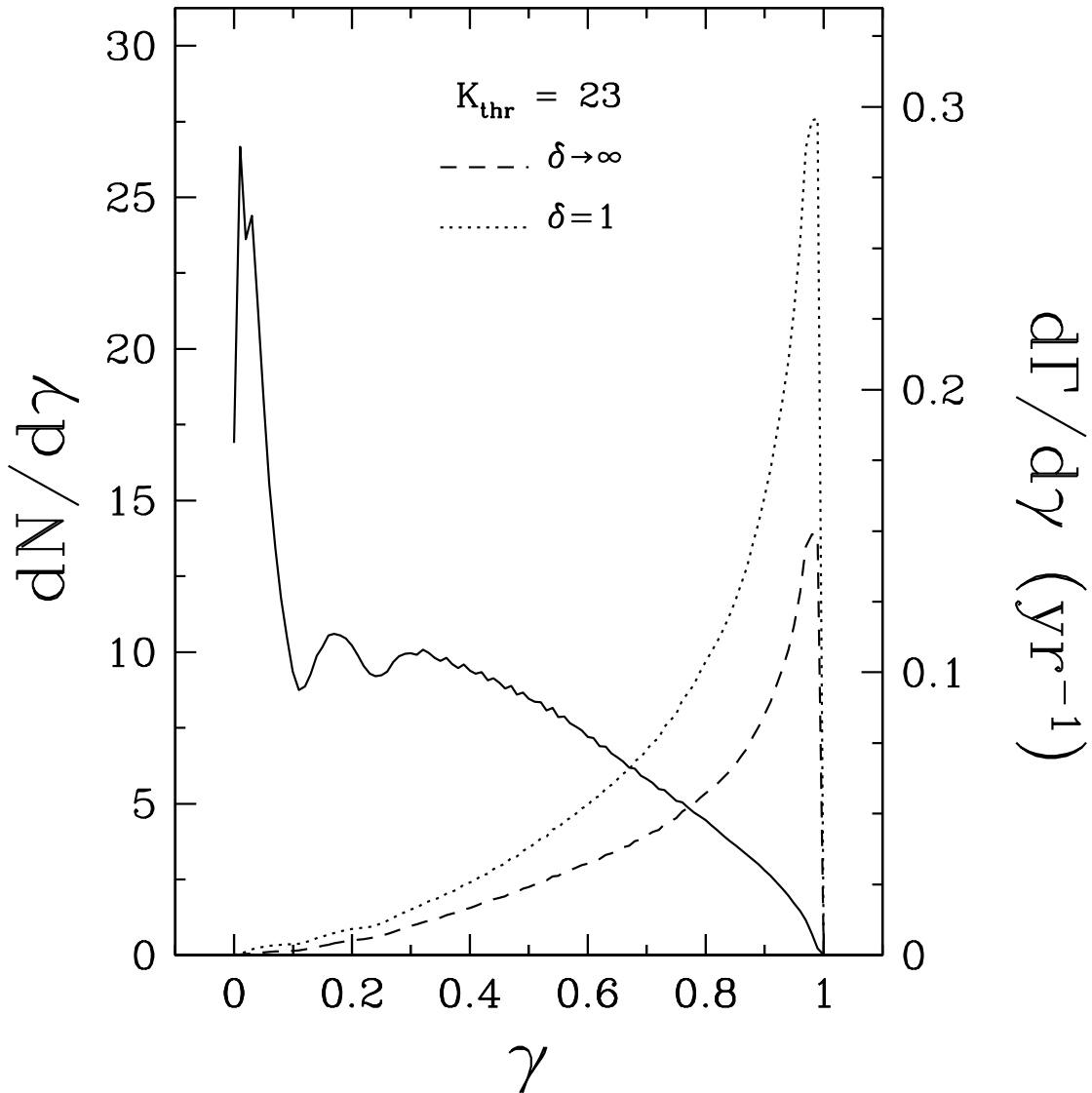


Fig. 4.— Comparison of the shear distributions of the rate of microlensing events for the cases when caustic crossing is required (dashed line), and when a peak magnification of at least a factor of two relative to the magnification by Sgr A\* is required (dotted line). In the latter case the total rate (area under the distribution) is almost doubled compared to the caustic crossing case. The solid line is the same as in the upper panel in Figure 2.